# In-situ measurement of the acoustic performance of a nearly-enclosed barrier prototype on an existing line in the urban rail transit system

Qiutong Li, Yanyun Luo, Denis Duhamel, Honore Yin, Y. Liu, Zhehao Zhu

# In-situ measurement of the acoustic performance of a nearly-enclosed barrier prototype on an existing line in the urban rail transit system

Qiutong LI[a], Yanyun LUO[b], Denis DUHAMEL[c,*], Honore YIN[c], Y. LIU[a], Zhehao ZHU[c]

[a]*Shanghai Research Institute of Materials, Shanghai, 200437, P.R. China*
[b]*Institute of Rail Transit, Tongji University, Shanghai 201804, P.R. China*
[c]*Ecole des Ponts ParisTech, UGE, CNRS, Laboratoire Navier, 6-8 Av. Blaise Pascal, 77455, Marne La Vallée, Cedex 2, France*

**Abstract**

The acoustic performance of a nearly-enclosed prototype meant to attenuate urban rail transit (URT) noise was measured in situ on an existing line. The prototype is constructed on a viaduct on Line 1, Ningbo, China, with a 2-meter-wide opening at the top. A series of measurements while trains passed by were carried out with twelve receiver positions at the site without and with the prototype. Train speeds were measured using a piezoelectric acceleration sensor located on a rail foot. By correcting pass-by levels for train speed, the measured results show that the nearly-enclosed prototype provides an attenuation with a maximum of 17 dB(A), and a minimum of 6 dB(A). One-third octave band spectrum analysis shows that the insertion loss specific to rolling noise yields on average more than 15 dB. Furthermore, comparisons between measured and predicted results by using 2.5-D boundary element method (2.5-D BEM) show that both of the employed PC and PMMA sheets could not provide sufficient transmission loss for the prototype in a real situation. Nevertheless, the nearly-enclosed prototype is effective against rolling noise for the URT system.

*Keywords:* Noise barrier, Urban rail transit, In situ measurement, Boundary element method

## 1. Introduction

Due to the rapid urbanization in China, Urban rail transit (URT) systems have entered a phase of rapid expansion. However, because of their exposure to the environment, vibration and noise pollution generated by elevated lines has become an urgent and serious problem. If this cannot be sufficiently solved, the development and use of the land space along the lines will be severely affected [1, 2]. To tackle this noise pollution, one of the effective ways is noise barrier [3–6]. Basically, there are three types on the existing lines in China: conventional straight barrier, half-enclosed barrier and fully-enclosed barrier. Among them, fully-enclosed barriers are the most effective at reducing URT noise. For fire safety, an opening is designed at the

*Corresponding author
*Email address:* denis.duhamel@enpc.fr (Denis DUHAMEL)

top of fully-enclosed barrier. Hence in this work we call it the "nearly-enclosed" barrier. A nearly-enclosed barrier constructed on a viaduct can contain almost all sound energy inside the barrier, and therefore is able to acoustically isolate residential buildings and industries from URT noise.

Previous studies [7–11] on nearly-enclosed barriers mostly used numerical modeling methods to evaluate the efficiency. Most are ray tracing method with software Cadna/A and statistical energy analysis (SEA) with software VA One, although boundary element method (BEM) is widely used in the prediction of barrier efficiency [6, 12–14]. Since the insertion losses were predicted typically over 20 dB(A), nearly-enclosed barriers are applicable to many urban lines in different cities. However, little is known about nearly-enclosed barriers through in-situ measurements. Coincidentally a fully-enclosed barrier was built on the Shenzhen-Maoming Railway line for the first time in China. X. Wu et al.[15] measured insertion loss of the fully-enclosed barrier by using indirect measurement method according to the norm ISO 10847-1997. The results showed that when the train speed was not higher than 132 km/h, the insertion loss generated by the concrete barrier could be on average 16-18 dB. However, for assessing the actual performance on reducing URT noise, it seems necessary to carry out in-situ measurements in a real situation.

In urban environments along URT lines, many sources of noise coexist during a train pass-by, including wheel/rail rolling noise, as well as vehicle noise and pantograph noise. It is generally believed that rolling noise generated by wheel/rail interaction is the predominant source in URT systems, with a feature of incoherent line source. However, many studies [6, 16–18] used one or two coherent line sources as an alternative in 2-D numerical models. A few types of sound source have already been studied [19, 20], and it has been emphasized that the coherent line source overestimated the efficiency and therefore to find a numerical method using incoherent line source but saving computation time seems critical in this context. A 2.5-D BEM approach, proposed by Duhamel [21, 22], is appropriate for this purpose. The main idea of this approach is to solve the sound pressure fields created by point or incoherent line sources by using a Fourier-type formulation to transform the 2-D BEM results. With the help of the 2.5-D BEM method, the insertion losses of a barrier for URT noise can be predicted though with large computational cost.

In this work, the performance of a nearly-enclosed barrier prototype meant to attenuate URT noise for the surroundings is measured in situ on an existing line. The selection of the measurement sites and the design of the prototype are introduced at first. Then the measurement method and the implementation are presented. The measured results are analyzed in relation to train speed in order to evaluate exactly the insertion loss. Comparisons with 2.5-D boundary element method (2.5-D BEM) predictions are made to reasonably explain the in-situ acoustic performance of the nearly-enclosed prototype.

## 2. Preparatory work

### *2.1. Selection of measurement sites*

The measured prototype is a typical nearly-enclosed barrier with a length of 420 m. The measurement site was selected close to the midpoint of the length of the barrier. The measured line is next to a four-lane road which separates the highly protected area from the lines (see Figure 1), with many cars and trucks passing by. On the other side there is a river between factories and the measured lines. In terms of the acoustic nature of the ground, the surface of ground is asphalt, and therefore it was assumed as acoustic rigid surface. Green vegetation covered the ground under the bridge and therefore the SPL at receiver M1-1 was partly absorbed by the green vegetation. Due to the totally reflective surface of bridge piers, the measurements were conducted in the middle of a bridge stride, between two piers. When measuring, cars and trucks were prevented from passing through the measured sites to reduce the influence of traffic noise. Given the complexity of the environment, it is essential to pay attention to the interference of background noise.

In addition to background noise, track structures also have a major influence on the emission of URT

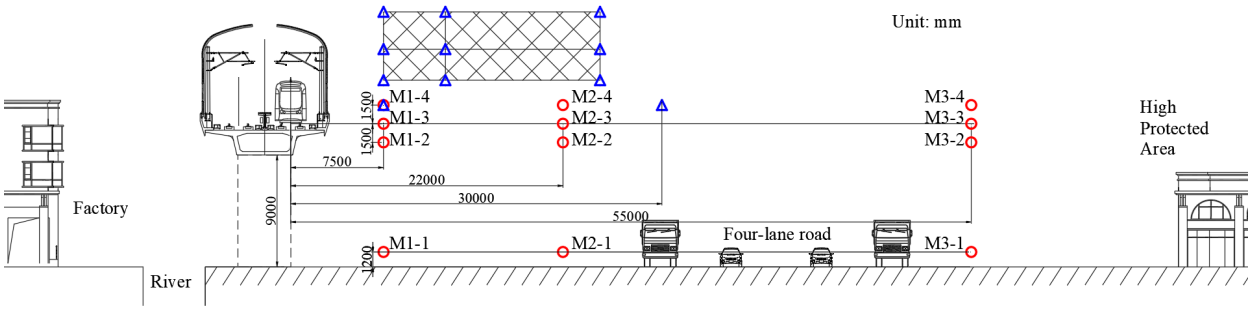


Figure 1: The configuration of the site with the nearly-enclosed prototype ( Twelve red circles: receiver positions; blue triangles: recommended positions stated in the ISO and European norms)

noise, and therefore would bias the acoustic performance evaluation of a barrier. On the selected site, floating slab tracks (FSTs) have been constructed on the viaduct. It is theoretically and experimentally proved that FSTs effectively reduced structure-borne noise radiated from the viaduct [23–25]. With the low-frequency characteristics of the structural noise, the measured insertion losses at low frequencies must be overestimated compared with those for the prototype itself. On the other hand, since most of the rail vibration energy is isolated by the FSTs, it may react on the rail vibration. And therefore it will make some contributions to the emission of rolling noise. As a consequence, the influence of the FSTs is worthy of great attention.

Another measurement site was required and determined where there is no barrier but several similar environmental factors as well as the train speed being almost identical to the aforementioned one. To

distinguish these two sites, we use "a site without a barrier" and "a site with a barrier" to describe them afterwards. Figure 2 displays these two sites. At the site without a barrier (see Figure 2(b)), the receiver

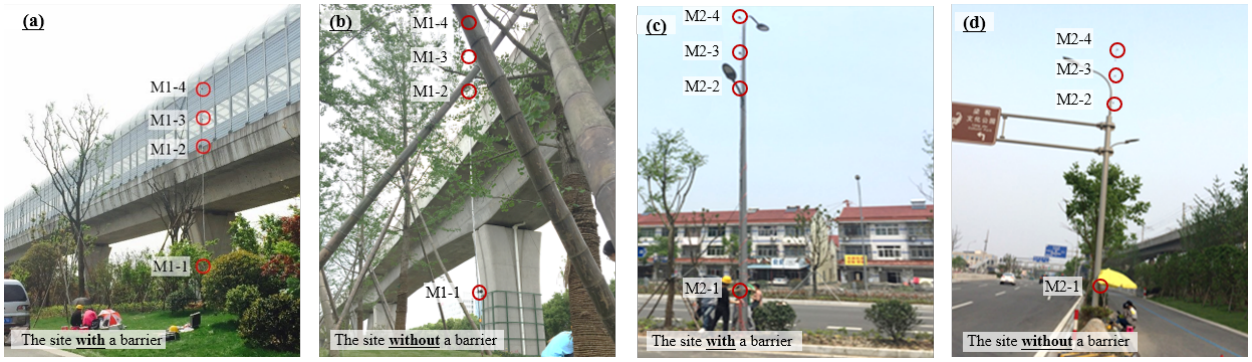


Figure 2: The scenes of the measurement sites: (a) receiver column M1- at the site with a barrier; (b) receiver column M1- at the site without a barrier; (c) receiver column M2- at the site with a barrier; (d) receiver column M2- at the site without a barrier.

M1-1 was partly covered by the green vegetation, as well as that for the site with a barrier (see Figure 2(a)). Furthermore, at both sites, the pole with receiver column M2- was tied to the lamppost (see Figure 2(c) & (d)) , whereas that with receiver column M3- was tied to the distant one. The surfaces of ground close to M2- & M3- are also asphalt, and the green plants close to the lamppost also located at both sites. Figure 3 illustrates locations of these two sites on the flat map. It can be seen that both measured sites are on the

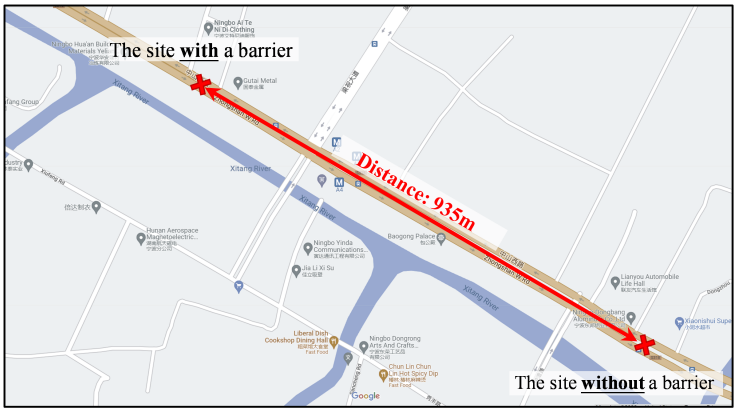


Figure 3: The locations of two measurement sites on the flat map.

same road close to the line, and the distance between them is less than 1 kilometer. Consequently, there is no barrier at the equivalent site, but several similar environmental factors are almost identical to the site where there is a nearly-enclosed barrier. Note that there is no presence of FST on the site without a barrier. It means that on the site with no barrier, the structural-borne noise of the viaduct cannot be reduced by the FST. Hence the measured insertion losses in our case would be the combination effect of the prototype

and the floating slab tracks.

### *2.2. The design of the prototype*

A schematic cross section of the prototype is shown in Figure 4, composed of several parts: one-side

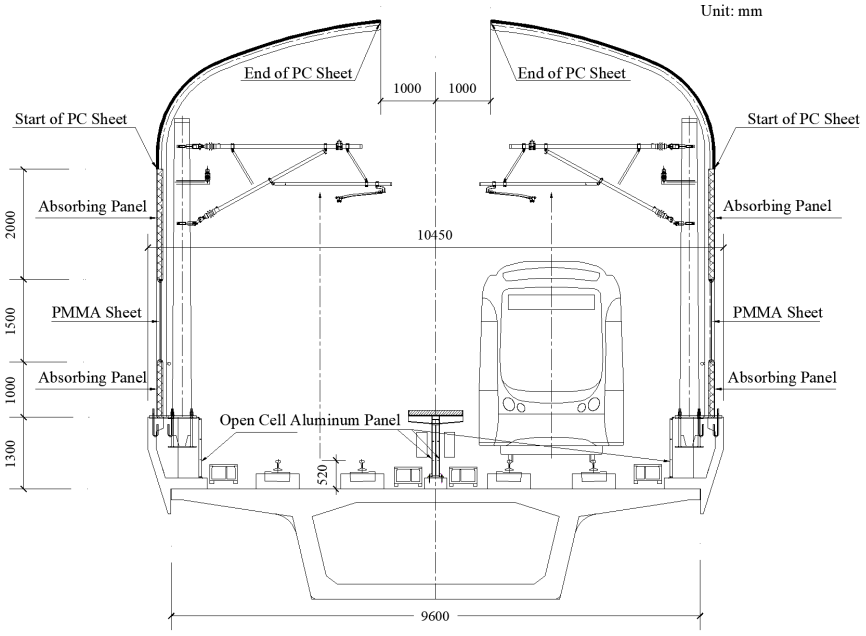


Figure 4: A cross section of the prototype

open-cell Aluminum panels located on the inner surface of two flanges, two-side open-cell Aluminum panels on the central T-shape passageway, and arched parts fixed on two sides of the viaduct. Each arched part is an assembly of two sound absorption panels, a PMMA sheet, a PC sheet and welded steel frameworks. The absorption panels, jagged and filled with $48kg/m^3$ glass wool, have a thickness of 60 mm. The transparent PMMA sheet with a thickness of 15 mm is designed for reducing drivers' fatigue, while the 6.5-mm-thick PC sheet is utilized to offer more flexibility for the shape and efficient sound insulation capability. The open-cell Aluminum panels are adopted for absorbing rolling noise, each made up of a 4-mm-thick open-cell aluminum foam panel, a 50-mm-thick cavity and a 1.5-mm-thick backboard.

### *2.3. Measurement method*

#### *2.3.1. Arrangement of receiver positions*

As stated in the ISO and European norms [26, 27], the measured receiver positions are recommended to be forming a grid (marked by blue triangles in Figure 1), so as to present the acoustic performance of a barrier on the bright zone, transition zone, and shadow zone behind it, respectively. One of our previous studies [28] showed that this gridded measurement technique enabled a good visualization of the acoustic

performance. However in this case, the bright and transition zone behind the nearly-enclosed prototype were too high to reach and the highly protected areas are mostly in its shadow zone. Moreover, the microphones could not be fixed stably since disturbances were frequent and unavoidable at the top of such a high support. Thus, as a compromise, some of the receivers were positioned below the height of the track instead. The furthest receiver column (M3-) was considered to be placed much closer to the highly protected area than the recommended position (see Figure 1, the blue triangle 30 meters away from the source), since the nearly-enclosed barrier was designed for protecting this area from the urban rail noise.

Based on these considerations, the receiver positions were eventually determined and are marked by red circles in Figure 1. The name of each receiver begins with "M". The first number represents the column number which is smaller as the receiver gets closer to the source, whereas the second number indicates the row number which is smaller as the receiver gets closer to the ground. A symbol like "M1-" "M-1" which will be seen in later sections designates, for example, all the receivers in the first column or the first row, respectively. In summary, we have twenty-four different configurations of measurements depending on twelve receiver positions at sites with and without a barrier.

Sound pressure signals were recorded by four B&K microphones (Type 4189, the corresponding response frequency ranges from 20 Hz to 20 kHz). They were omnidirectional and protected by windscreens, as shown in Figure 5(a). The signals were sampled at 51.2 kHz to avoid message distortion. In addition, the microphones were mounted in the grazing position on the standing poles due to signal contamination caused by the microphone safety grid [29].

*2.3.2. Speed measurement from vibration signals*

Train speed is one of the important parameters that influences the pass-by sound pressure level. It is well known that train speed can be measured by the length of a train and the duration of its pass-by. However, due to the presence of barriers the general method to measure speed is worthless. One approach, as detailed in [30], is to use an extra microphone close to the track to calculate speed by the formula $v = d/\Delta t$ with $\Delta t$ the time intervals between the passage of the first and the last bogie, and $d$ the distances between the corresponding bogies. In this measurement, train speeds were calculated from measuring the time histories of vertical acceleration level of the rail ($AL_{eq,T}$). The acceleration signals were recorded by a piezoelectric acceleration sensor (range: 500g) shown in Figure 5(b). The signals were sampled at 5120 Hz based on the Nyquist Theorem. The records were started automatically two seconds ahead of a trigger from the bump generated by the first bogie pass-by, in sync with the recordings of sound pressure signals.


(a) The microphones (b) The piezoelectric acceleration sensor

Figure 5: The apparatus used at the site with the prototype

### *2.4. Implementation*

The measurements at the sites without and with a barrier were conducted on sunny days six days apart. The wind direction was southeast whereas the wind speed went to less than 5.4m/s for both two measurement days. The percentage of wind speed in sound speed was just about 1.5% and thus the effect of wind speed to the sound could be ignored. The temperature for the first day differed by only $1-2\,^{\circ}\mathrm{C}$ from that for the second day. There was no rain so that the humidity was relatively low. Thus, the meteorological conditions were not significantly different between the two measurement days. Due to a limitation on the number of apparatuses, four microphones were fixed on a long upright pole to simultaneously measure sound pressure at the same horizontal distance from the source but different vertical distances, e.g., at the same time measuring sound pressure at receiver M1-4, M1-3, M1-2 and M1-1 (shown in Figure 5(a)). Then this pole was moved further from the source, to record sound at the other two horizontal distances. All the measurements were performed only for the duration of trains passing through the measured cross-section. At each horizontal distance (e.g., M1-), the measurement was repeated 10 times or more to ensure the statistical representativeness of the sample. When measuring, cars and trucks were prevented from passing through the measured sites to reduce the influence of traffic noise. For each microphone, the background noise was measured at each position when there was no train in the measured section. The background noise was measured for 30 seconds. In addition, all the apparatus including acoustic amplifiers, electrical charge amplifiers, sound pressure collecting equipment and A/D data collection cards met the requirements of EN 61672-1 and the microphones complied with IEC 61672 class 1.

## 3. Measured results and discussion

During the measurement, trains passed through the two measured sections with different speeds. Therefore, the speed dependence of rail vertical vibration and sound pressure at each receiver position was discussed

at the beginning of this section. Then, by using the dependence curves, the measured sound pressure signals were speed-corrected to analyze the spatial distribution and the spectrum, in order to present a comprehensive view of the measured noise characteristics. The acoustic performance of the barrier prototype was eventually investigated.

### *3.1. Train speed dependence*

#### *3.1.1. Train speed dependence of rail vertical acceleration*

The train speed for each record was calculated through the measured time histories of rail vibration acceleration level $AL_{\mathrm{eq,T}}$. To identify the pass-by of every bogie, the recorded signals were averaged at 100 ms intervals. Figure 6 shows two examples of the time histories for $AL_{\mathrm{eq,T}}$. It can be seen that the acceler-

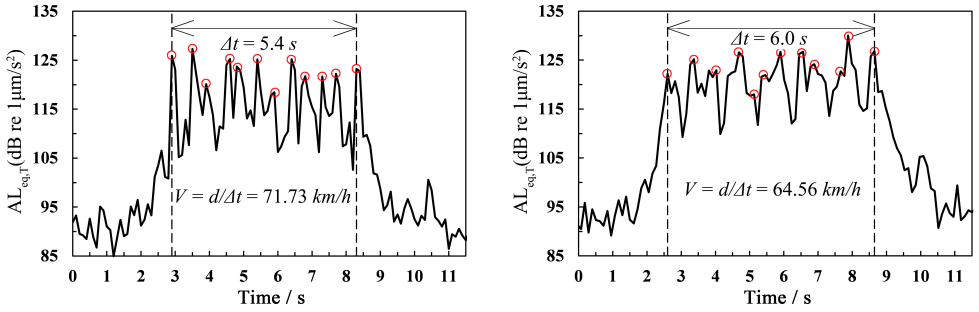


(a) At the site without a barrier

(b) At the site with a barrier

Figure 6: Examples of time histories for the rail vertical acceleration$AL_{\mathrm{eq,T}}$
(Red circles: peaks caused by the pass-by of bogies.)

ation level increases gradually in the first 3 seconds, then raises sharply for about 6 seconds, and finally the acceleration level decreases back to the level as high as the beginning. This variation trend presents a vivid description of a train approaching the measured section, passing through and leaving.

Figure 6 also presents twelve sharp peaks during a train pass-by. Since each standard train on this line has twelve bogies fixed, it is reasonable to suppose that these peaks were caused by the pass-by of bogies. As the distance between the pass-by of the first and last bogie is $d = 107.6m$, the train speed for each record can be calculated by the formula $V = d/\Delta t$ with the time history of $AL_{\mathrm{eq,T}}$, assuming it is constant. $\Delta t$ denotes the time period from the first peak to the last one (e.g. see Figure 6).

By averaging twelve peak values of $AL_{\mathrm{eq,T}}$ for each record, the mean $AL_{\mathrm{eq,T}}$s were plotted as a function of the logarithm of the corresponding train speed, as shown in Figure 7. It displays that the train speed varies between 55 km/h and 75 km/h at both sites, and the $AL_{\mathrm{eq,T}}$ increases with train speed. The slopes between the acceleration level and the logarithm of train speed are 32 and 31 for the site without a barrier and with a barrier, respectively, and the coefficients of correlation are 0.84 and 0.73, respectively. Besides, train speeds at the site without a barrier are concentrated in a range above 70 km/h, whereas most of those

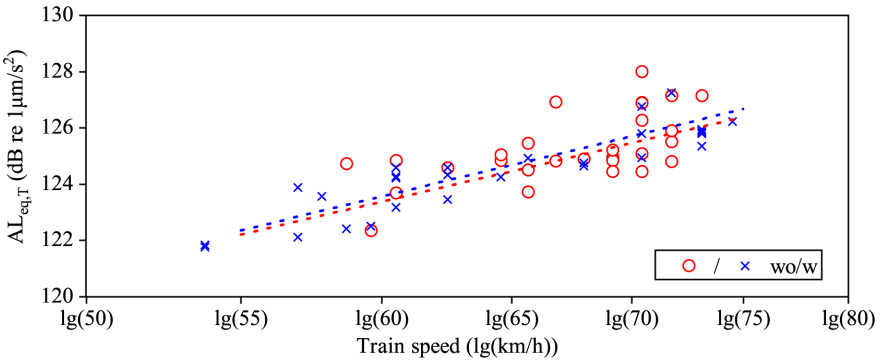


Figure 7: The relationship between $AL_{\mathrm{eq,T}}$ and train speed at both sites
(Red circles: the mean $AL_{\mathrm{eq,T}}$ at the site without a barrier, blue crosses: the mean $AL_{\mathrm{eq,T}}$ at the site with a barrier, red curve: the regression curve for the site without a barrier, blue curve: the regression curve for the site with a barrier.)

at the site with a barrier are less than 65 km/h. This is due to the blockage of the nearly-enclosed barrier which caused the rail traffic to slow.

By using the least squares estimation method, two linear regression models were obtained for the relationship between $AL_{\mathrm{eq,T}}$ and train speed at both sites, and are represented by dotted curves in Figure 7. Obviously, with the same speed, the blue dotted curve is slightly higher than the red dotted curve. The difference between these two curves could be attributed to the influence of the floating slab track as introduced in Section 2.1. However, the influence could be negligible since the differences are always less than 0.5 dB. Thus, there is no need to pay attention to the influence of the FSTs on rolling noise. In addition, those significant deviations between the regression curves and the measured results are probably due to wheel defects, rail defects and the variation of train load.

### *3.1.2. Train speed dependence of measured noise*

Figure 8 presents time histories of A-weighted sound pressure level for receiver M1-4 at both sites, which were recorded in sync with the examples of $AL_{\mathrm{eq,T}}$ in Figure 6. It can be seen that the pass-by level increases considerably when a train was passing through the measured section at the site without a barrier, whereas at the site with a barrier there is a small increase. These increases are almost synchronous with those for the rail vibration acceleration levels, which can be explained appropriately by a train pass-by. Thus, the measurement technique to measure rail accelerations for determining the time period of a train pass-by and the train speed is accurate and reasonable, which can be generalized to the in-situ measurements.

The equivalent continuous A-weighted sound pressure level during the train passing by $L_{\mathrm{Aeq,pass}}$ is introduced to estimate the measured noise [26, 27], as given by

$$L_{\mathrm{Aeq,pass}} = 10\log_{10}\left[\frac{1}{T_p}\int_{t_1}^{t_2}\frac{p_A^2(t)}{p_0^2}dt\right] = 10\log_{10}\left[\frac{1}{N}\sum_{n=1}^{N}\frac{p_A^2(n)}{p_0^2}\right] \quad (1)$$

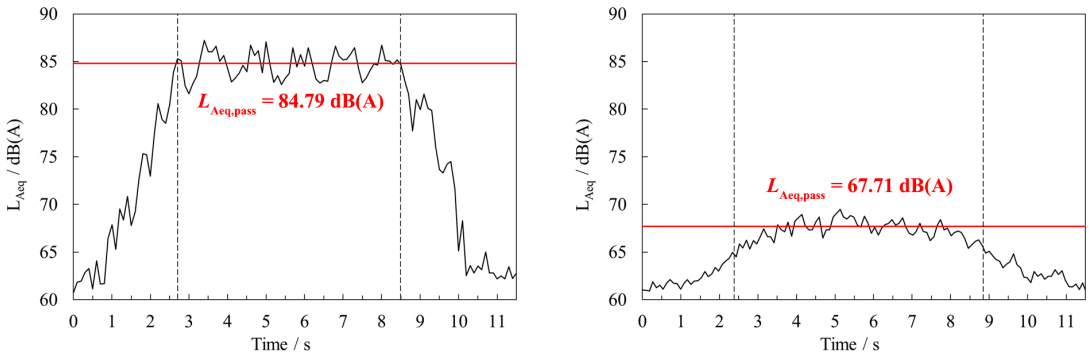


(a) At the site without a barrier

(b) At the site with a barrier

Figure 8: Examples of time histories for A-weighted level measured at M1-4, which were recorded in sync with the examples for $AL_{eq,T}$ shown in Figure 4 (The two dotted vertical lines in each sub-figure represent the starting point and the ending point, respectively.)

where $T_p$ denotes the duration of a train passing through, $t_1$ is the starting time when the first car head enters the measured cross-section whereas $t_2$ is the ending time when the last car tail leaves. $p_{\mathrm{A}}(t)$ denotes A-weighted instantaneous sound pressure at $t$ second, and $p_0$ is the reference sound pressure (usually $20\mu Pa$). The last term is a discretization, where $N$ denotes the sampling points. This discretization term was employed for the measurement analysis to handle the measured data.

Figure 8 marks the $L_{\mathrm{Aeq,pass}}$ by red horizontal lines. The $L_{\mathrm{Aeq,pass}}$ provides the mean characteristics of the pass-by level in the time history, which can be a good indicator to describe the measured noise. Figure 9 illustrates the relationship between train speed and $L_{\mathrm{Aeq,pass}}$ for M1-4 at both sites. Their relationship is

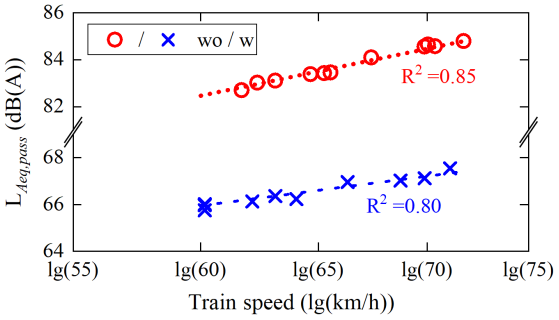


Figure 9: The relationship between $L_{\mathrm{Aeq,pass}}$ for M1-4 and train speed (Red circles: the $L_{\mathrm{Aeq,pass}}$ at the site without a barrier, blue crosses: the $L_{\mathrm{Aeq,pass}}$ at the site with a barrier, red curve: the regression curve for the site without a barrier)

properly performed by a linear regression model, given as,

$$L_{\mathrm{Aeq,pass}}(V) = \alpha \log_{10}(V/V_{\mathrm{ref}}) + L_{\mathrm{Aeq,pass}}(V_{\mathrm{ref}}) \tag{2}$$

where $V_{\mathrm{ref}}$ denotes the reference speed and $L_{\mathrm{Aeq,pass}}(V_{\mathrm{ref}})$ is the corresponding reference level. Assuming that the reference speed equals to 65 km/h, the calculated results for the reference level $L_{\mathrm{Aeq,pass}}(V_{\mathrm{ref}})$,

the slope $\alpha$ and their uncertainties for each receiver at the site without and with a barrier, are calculated and given in Table 1. It is noteworthy that the slope $\alpha$ for all the receivers at the site without a barrier

Table 1: The reference level $L_{\mathrm{Aeq,pass}}(V_{\mathrm{ref}})$, the slope $\alpha$ and their uncertainties for each receiver at the site without and with a barrier ($V_{\mathrm{ref}} = 65km/h$), and the speed-corrected insertion loss for each receiver(unit: dB(A))

| Receiver | Site type | $L_{\mathrm{Aeq,pass}}(V_{\mathrm{ref}})$ | coefficient $\alpha$ | The estimate for the insertion loss |
|---|---|---|---|---|
| M1-4 | Without a barrier | 83.39±0.20 | 31.60±4.95 | 16.69±0.40 |
| | With a barrier | 66.70±0.20 | 18.84±3.72 | |
| M1-3 | Without a barrier | 72.90±0.25 | 29.21±5.57 | 9.84±0.47 |
| | With a barrier | 63.06±0.22 | 18.34±4.17 | |
| M1-2 | Without a barrier | 73.04±0.39 | 28.54±6.77 | 8.35±0.60 |
| | With a barrier | 64.69±0.20 | 18.84±3.72 | |
| M1-1 | Without a barrier | 67.85±0.20 | 27.10±8.17 | 6.33±0.67 |
| | With a barrier | 61.51±0.12 | 18.72±3.13 | |
| M2-4 | Without a barrier | 73.45±0.63 | 29.18±8.48 | 12.70±0.96 |
| | With a barrier | 60.75±0.33 | 19.54±5.19 | |
| M2-3 | Without a barrier | 67.45±0.59 | 27.51±7.90 | 9.79±0.95 |
| | With a barrier | 57.67±0.36 | 21.46±5.72 | |
| M2-2 | Without a barrier | 70.61±0.57 | 30.56±8.08 | 8.88±0.85 |
| | With a barrier | 61.73±0.28 | 21.87±4.86 | |
| M2-1 | Without a barrier | 71.62±0.49 | 26.98±6.95 | 9.16±0.84 |
| | With a barrier | 62.46±0.35 | 20.23±5.48 | |
| M3-4 | Without a barrier | 69.57±0.53 | 28.34±9.47 | 8.68±0.69 |
| | With a barrier | 60.89±0.16 | 17.15±3.00 | |
| M3-3 | Without a barrier | 64.17±0.50 | 27.54±9.07 | 8.03±0.95 |
| | With a barrier | 56.14±0.45 | 18.22±5.63 | |
| M3-2 | Without a barrier | 68.35±0.40 | 26.59±7.67 | 7.64±0.85 |
| | With a barrier | 60.72±0.45 | 19.66±5.75 | |
| M3-1 | Without a barrier | 73.03±0.47 | 30.69±8.91 | 12.07±0.72 |
| | With a barrier | 60.95±0.25 | 18.53±3.86 | |

are close to the value of 30 that is commonly used in the prediction formula for rolling noise[31]. The regression model for M1-4 at the site without a barrier is also plotted by a red dotted curve in Figure 9. The correlation coefficient $R^2$ between the measured (the red circles) and predicted results (the red dotted curve) equals 0.85, which suggests that the measured noise was indeed radiated mostly from rolling noise. At the site with a barrier, the slope $\alpha$ for all the receivers are nearly 20, which indicates that the presence of the nearly-enclosed barrier can directly affect the relationship between train speed and the $L_{\mathrm{Aeq,pass}}$ in the surroundings, reducing the speed dependence but maintaining linear characteristics.

### *3.2. Background noise*

Background noise may have a serious interference on URT noise, particularly for the receivers far from the lines. In this measurement, the distances between source and receiver for the receivers in M3- are over 55 meters, much larger than those for other receivers. Hence the measured $L_{\mathrm{Aeq,pass}}$ for the receivers in M3- could be relatively less affected by the train pass-by, but influenced more seriously by background noise. To make it clear, we made a comparison between the measured $L_{\mathrm{Aeq,pass}}$ and the background noise $L_{\mathrm{Aeq,bg}}$ for the receivers in M3- at the sites without and with a barrier, respectively, listed in Table 2. One can notice that the differences for each receiver at the site with a barrier are much smaller than those at the site without a barrier. Among all the differences listed, the minimum is 12.36 dB(A) for M3-3 at the site with a barrier. ISO 10847-1997 [26] states that the level of background noise should be 10 dB or more below those obtained from measured signals. Calculated by A. Jolibois et al. in [30], the minimum difference in level was 9 dB when the error on the insertion loss was less than 0.5 dB. Therefore, in our case, the interference of background noise for the receivers in M3- is less than 0.5 dB, which is sufficient for the purpose of this work. Since background noise has much smaller influence on other measured receivers, we can conclude that the influence of background noise could be neglected in the following analysis.

Table 2: $L_{\mathrm{Aeq,pass}}$s, $L_{\mathrm{Aeq,bg}}$s and their differences for the receivers in M3- (unit: dB(A))

| Site | Receiver | $L_{\mathrm{Aeq,pass}}$ | $L_{Aeq,bg}$ | Difference |
|---|---|---|---|---|
| Without a barrier | M3-4 | 71.47 | 50.76 | 20.71 |
| | M3-3 | 66.04 | 44.99 | 21.05 |
| | M3-2 | 69.65 | 48.56 | 21.09 |
| | M3-1 | 75.07 | 48.84 | 26.23 |
| With a barrier | M3-4 | 60.91 | 47.16 | 13.75 |
| | M3-3 | 56.71 | 44.35 | 12.36 |
| | M3-2 | 60.94 | 47.72 | 13.22 |
| | M3-1 | 60.16 | 46.84 | 13.32 |

The spectra of background noise and the measured noise for M3-1 were also compared at the site without and with a barrier, respectively. As shown in Figure 10(a), the SPL in each one-third octave band for M3-1 is higher than that for background noise except from the band of 20 Hz. While at the site with a barrier, the SPL for M3-1 are all higher than the background noise. The frequency range stated in the ISO standard 10847-1997 is recommended from 50 Hz to 50 kHz [26], within which the differences between the measured results and the background noise are all over 10 dB. Hence, the error for the insertion loss will be less than 0.5 dB and it is acceptable to carry out the one-third octave analysis within the range of 50 Hz-5000 Hz.

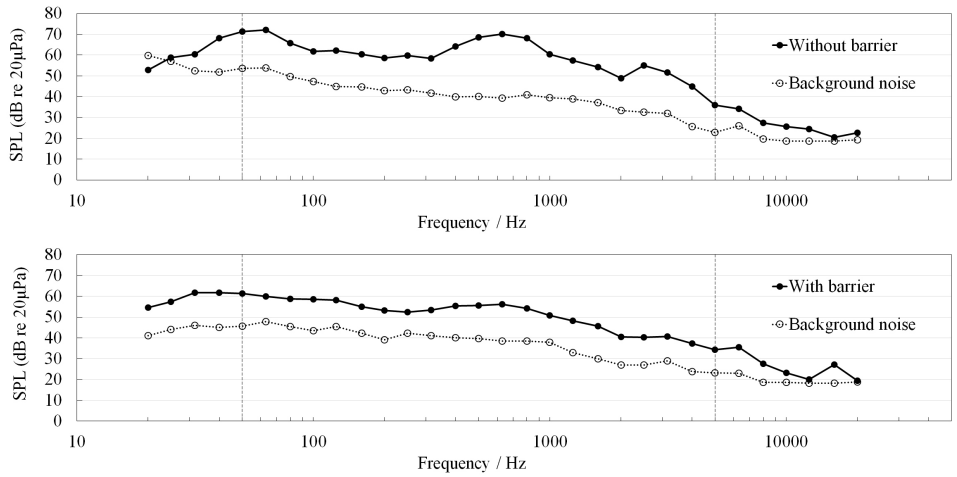


Figure 10: Sound pressure spectra for M3-1 in the frequency range of 20Hz-20kHz (upper: at the site without a barrier; lower: at the site with a barrier)

### *3.3. Measured noise characteristics*

#### *3.3.1. Spatial distribution*

The speed-corrected $L_{\mathrm{Aeq,pass}}$ for each receiver at both sites are arranged according to the receiver positions in reality, as shown in Figure 11. The source is assumed to be located on the left of this figure.

For the receivers at the site without a barrier (black bars), the maximum $L_{\mathrm{Aeq,pass}}$ is 83 dB(A) for

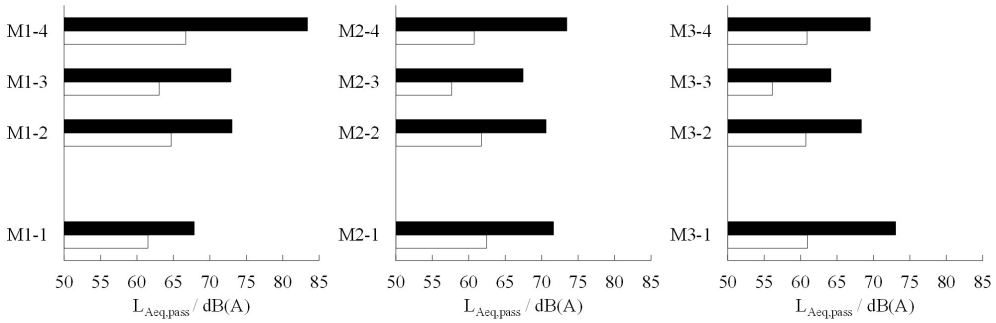


Figure 11: The speed-corrected $L_{\mathrm{Aeq,pass}}$ for each receiver (black bars: at the site without a barrier, white bars: at the site with a barrier). The source is assumed to be located on the left of this figure.

M1-4 due to the location higher than the top of the flange and at the closest horizontal distance among the receivers examined. The second maximum $L_{\mathrm{Aeq,pass}}$ is approximately 73 dB(A) for both M2-4 and M3-1. Attributed to the same height as M1-4, the $L_{\mathrm{Aeq,pass}}$ for M2-4 is relatively higher. Receiver M3-1 was also affected significantly by the URT noise, although it was located at the farthest vertical and horizontal source-receiver distance. Since the interference of background noise to the $L_{\mathrm{Aeq,pass}}$ for M3-1 could be ignored and receiver M3-1 was located the closest to the highly protected area, it is notable that the URT noise had

sufficient energy to transmit to the highly protected area. There are two reasons for the high level obtained at receiver M3-1. One is the barrier effect of the viaduct, and the other is the acoustic rigid road surface. Compared with other receivers in the row M-1, the barrier effect of the viaduct structure had less influence on the SPL at M3-1. Thus, the SPL at M3-1 was higher than those at M1-1 & M2-1. Compared with other receivers in the column M3-, the reflection effect of the road surface had more influence on the SPL at M3-1. Thus, the SPL at M3-1 was higher than those at M3-4, M3-3, M3-2 & M3-1. As these values are much higher than the limit value (70 dB(A)) stated on the Chinese norm GB 3096-2008 [32], it is absolutely necessary to reduce noise by effective measures.

For the receivers at the site with a barrier, the speed-corrected $L_{\mathrm{Aeq,pass}}$s are all acceptable since they are lower than the limit value 70 dB(A). As observed from the white bars in Figure 11, there is a similar pattern to the black bars that the speed-corrected $L_{\mathrm{Aeq,pass}}$ in each row (M-2, M-3 and M-4) decreases with horizontal distance increasing from the source. However, the $L_{\mathrm{Aeq,pass}}$s for the receivers in row M-1 remain at a level around 61 dB(A) with little difference. This variation trend differs completely from the change law in row M-1 at the site without a barrier, from which it can be deduced that the prototype had an effective influence on the $L_{\mathrm{Aeq,pass}}$ for the places close to the ground, reducing the second maximum level for M3-1 at the site without a barrier to the same as that for M1-1. Hence, the prototype was effective in preventing the URT noise from transmitting to the highly protected area.

### *3.3.2. Spectrum analysis*

One-third octave spectra for each receiver at the site without a barrier are shown in Figure 12. Each sub-figure presents three curves for the receivers in the same row. It can be seen that the measured noise has a significant low and mid- frequency characteristics. In the range below 200 Hz, SPL decreases with the increased frequency. From 200 Hz to 315 Hz, SPL remains on a high level. Then in the mid- frequency range of 315-1000 Hz, SPL at each receiver rises considerably with frequency, reaching to the global maximum at 500 Hz. In the range of 1000-2000 Hz, SPL decreases significantly with frequency. Finally at high frequencies (2000-5000 Hz), SPL at each receiver increases first and then decreases, with a local maximum at 2500 Hz. Note that the level in this range remains on a relatively lower level.

The high levels of measured noise at 50-200 Hz were attributed to the structural noise of the viaduct generated by trains passing by. Since the low-frequency noise attenuates slower than the high frequencies in air and thus transmits over longer distances, the SPLs at low frequencies were even higher than those of the mid frequencies at the receivers located farther from the source (the receivers in M3-). Besides, there are also high levels of measured noise at 315-1000 Hz and 2000-4000 Hz, with the global maximums at 500 Hz and local maximums at 2500 Hz. These frequency ranges were in good agreement with those of peaks measured by Javad S. and Araz H. for rolling noise of the train TM3-51 [33].

Figure 13 describes the one-third octave spectra for each receiver at the site with a barrier. The SPL

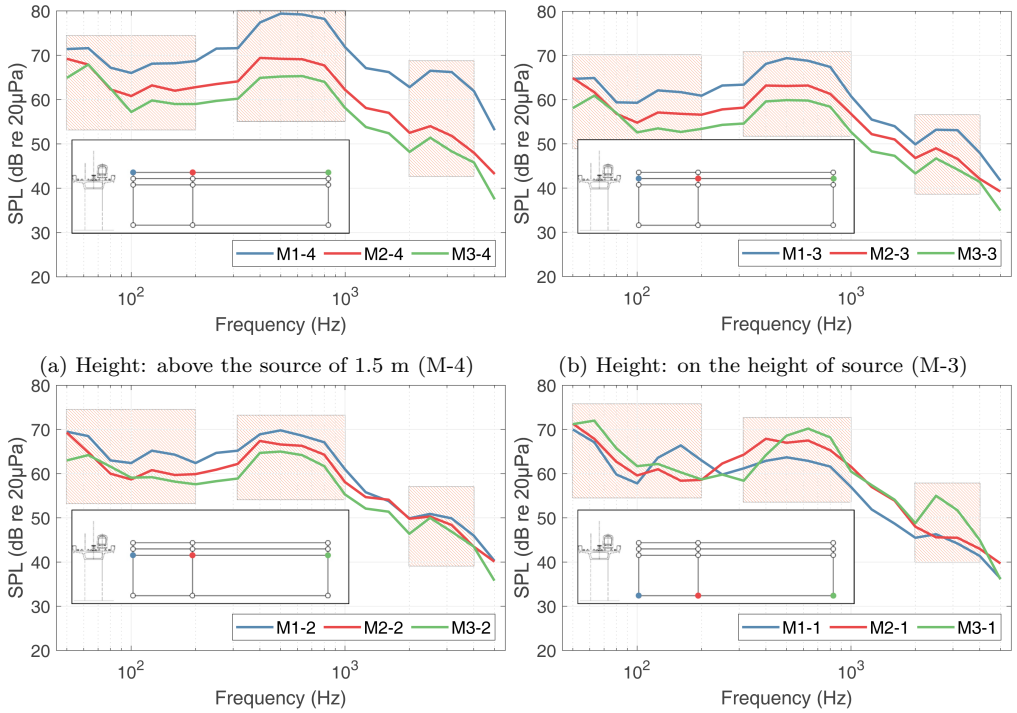


(a) Height: above the source of 1.5 m (M-4)

(b) Height: on the height of source (M-3)

(c) Height: below the source of 1.5 m (M-2)

(d) Height: 1.2 m above the ground (M-1)

Figure 12: Sound pressure spectra for the receivers at the site without a barrier

gradually decreases with the increased frequency, with maximums at low frequencies. The high levels at low frequencies are observed again because the reduction effect of the prototype was good for noise at mid- and high frequencies but bad for low-frequency noise. It is also worthy of note that the two measured increases in the range of 315-1000 Hz and 2000-4000 Hz in Figure 12 do not appear in this figure, which indicates that the nearly-enclosed prototype was effective in reducing the exposure to the measured rolling noise, though there is still a small peak in the band of 630 Hz.

### *3.4. Acoustic performance of the prototype*

#### *3.4.1. Spatial distribution*

Figure 14 shows the global insertion losses arranged according to the receiver positions, identical to the arrangement for the $L_{\mathrm{Aeq,pass}}$ in Figure 11. The maximum is over 15 dB(A) for receiver M1-4 where the $L_{\mathrm{Aeq,pass}}$ is also the highest at the site without a barrier. The second maximum is around 12 dB(A) for receiver M2-4 and M3-1 where the $L_{\mathrm{Aeq,pass}}$ are also the second highest at the site without a barrier. For other receivers the insertion losses of the nearly-enclosed barrier are less than 10 dB(A). With the decreased height above the ground, the insertion loss for the receiver in column M1- deceases significantly. The insertion loss for M1-1 is only 6.3 dB(A) since the $L_{\mathrm{Aeq,pass}}$ was reduced mainly by the barrier effect of the viaduct rather than the real noise barrier. As a result, the change law of the global insertion loss along

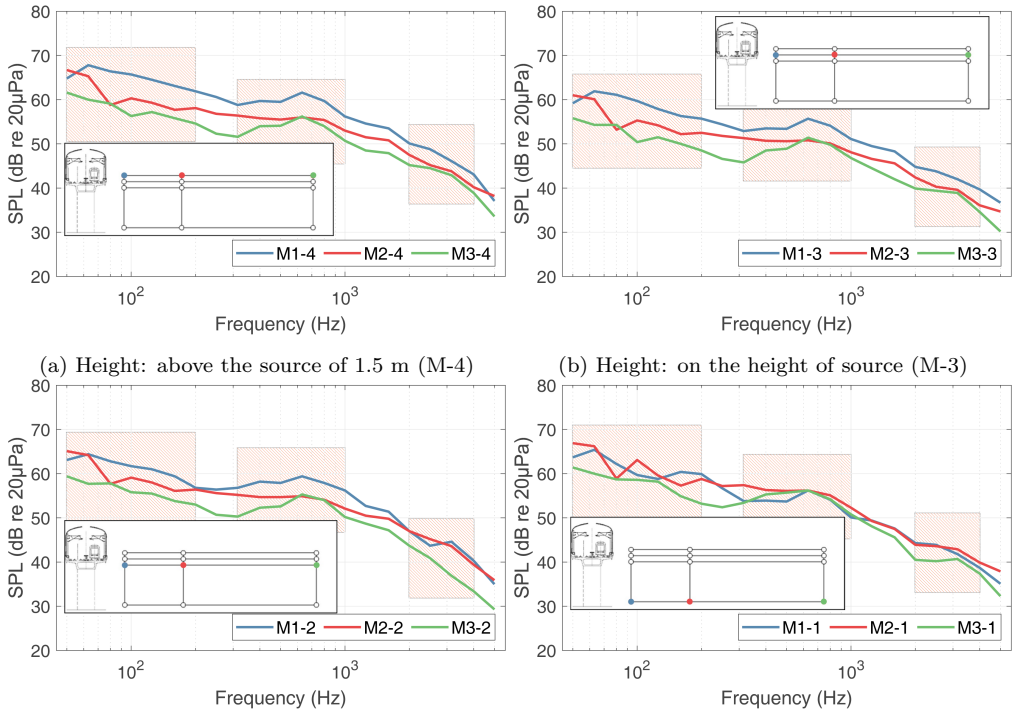


(a) Height: above the source of 1.5 m (M-4)

(b) Height: on the height of source (M-3)

(c) Height: below the source of 1.5 m (M-2)

(d) Height: 1.2 m above the ground (M-1)

Figure 13: Sound pressure spectra for the receivers at the site with a barrier

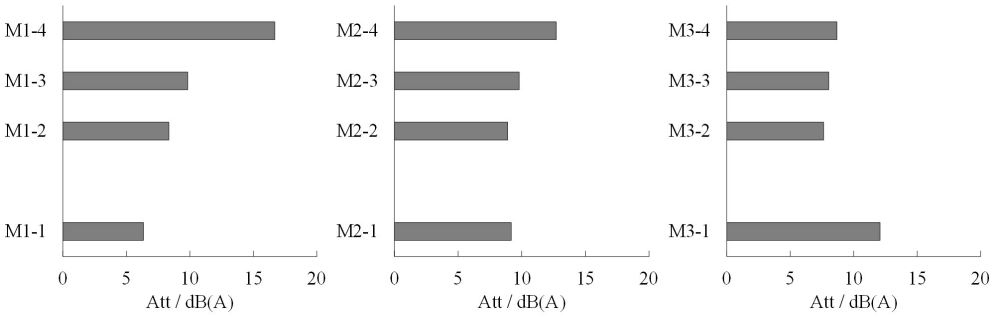


Figure 14: The global insertion losses in dB(A) for each receiver of the nearly-enclosed prototype

with the receiver position is almost the same as that of the $L_{\mathrm{Aeq,pass}}$ at the site without a barrier, which suggests that the nearly-enclosed prototype was indeed effective against the URT noise.

### *3.4.2. Spectrum analysis*

The one-third octave spectra of the insertion loss for each receiver position are carried out and shown in Figure 15.

Firstly, in view of the structure-borne noise from the viaduct structure, special attention needs to be paid to the low-frequency noise. The insertion loss for each receiver is around 5 dB from 50 Hz to 100 Hz.

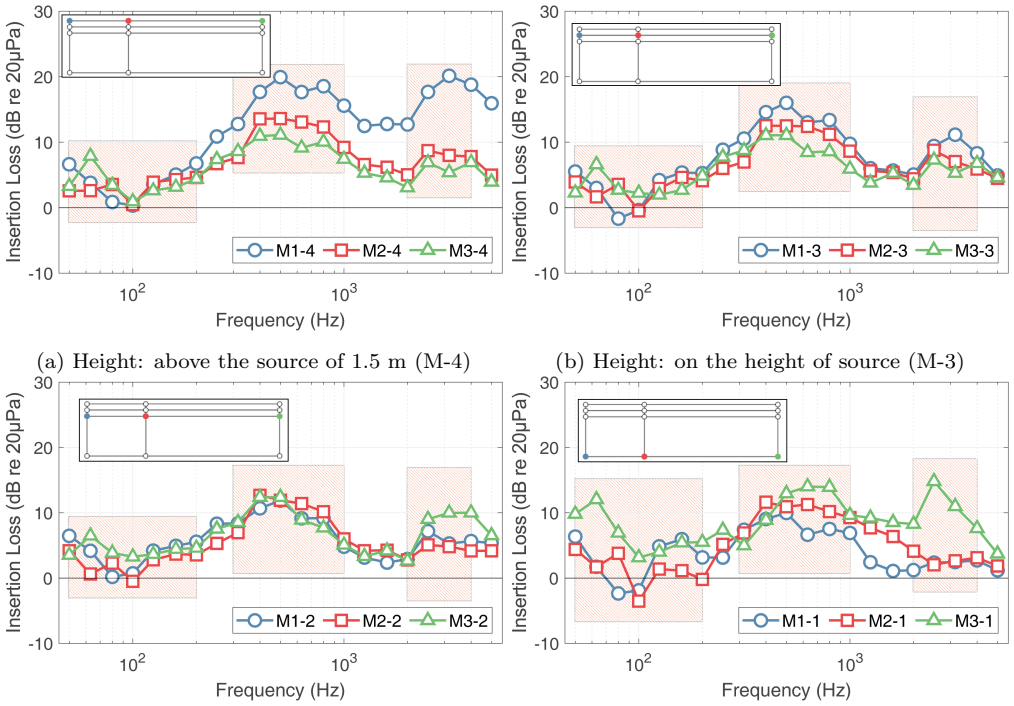


(a) Height: above the source of 1.5 m (M-4)

(b) Height: on the height of source (M-3)

(c) Height: below the source of 1.5 m (M-2)

(d) Height: 1.2 m above the ground (M-1)

Figure 15: The spectra of insertion losses for all the receivers examined

These remarkable low-frequency insertion losses are mostly attributed to the FST effect, since a conventional noise barrier is ineffective against low-frequency noise. In the range of 100-200 Hz, there is a minimum of a negative value at 100 Hz. The magnitude of the negative value is less than 5 dB, which indicates that the nearly-enclosed prototype had a harmful but not remarkable effect on the low frequencies. As we discussed in a previous article [34], the resonance effect caused by the open air cavity inside a nearly-enclosed barrier resulted in extremely high levels at the resonance frequencies. And with the help of the absorbent treatment, the harmful resonance effect was mitigated solely for the mid- and high frequencies. Hence these negative values at 100-200 Hz can be explained by the resonance effect of the nearly-enclosed prototype.

Secondly, the insertion losses in the frequency range of measured vehicle noise (315Hz-1kHz & 2kHz-4kHz) are discussed. As shown in Figure 15, in the range of 315-1000 Hz, the insertion losses for all the receivers are sufficiently high, with a maximum value of 20 dB at 500 Hz for M1-4. And the values for the receivers in column M1- are over 15 dB, whereas those for M2- and M3- are over 10 dB. To focus on another frequency range (2000-4000 Hz), the maximum is also found for M1-4 with the same value of 20 dB but at 3150 Hz. Unlike those high values in the range of 315-1000 Hz, the values for other receivers are less than 10 dB, except for M3-1. The high value of the insertion loss for M3-1 is 15 dB at 2500 Hz, due to the barrier effect of the viaduct and the acoustic rigid road surface. As a consequence, the nearly-enclosed prototype was sufficiently effective in reducing the measured vehicle noise.

## 4. A comparison with a 2.5-D BEM model

The geometries of 2.5-D BEM models were obtained from the configurations examined in the in-situ measurement, with the cross-section of the site without a barrier and the site with the nearly-enclosed prototype, respectively. Another model with the double-straight barrier without two top arched parts was built as well. Figure 16 shows the cross-sections of these three models. Two incoherent-line sources were

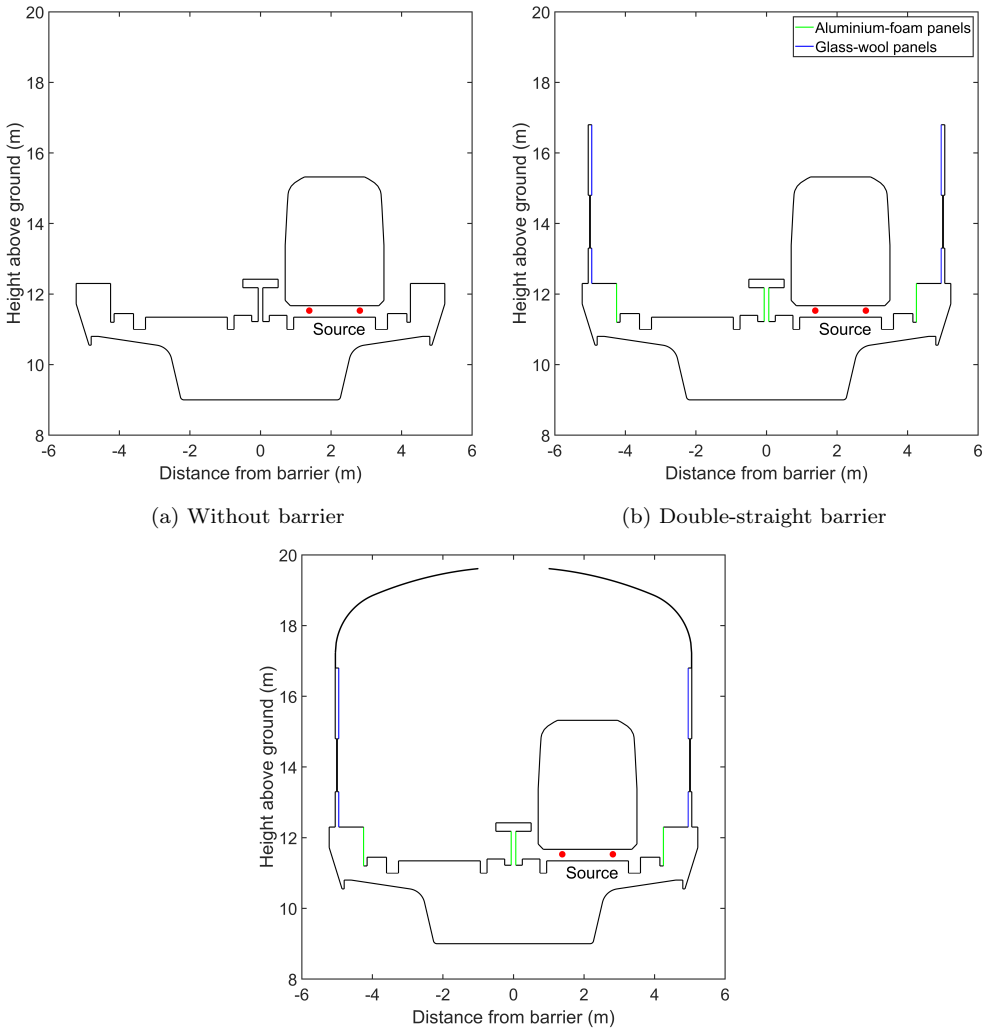


(a) Without barrier

(b) Double-straight barrier

(c) Nearly-enclosed barrier

Figure 16: Cross-sections of three 2.5-D BEM models calculated in the comparison with measured results

assumed located at the positions of the wheel-rail interactions (red dots in Figure 16). The blue curves represent the absorbing panels with glass wool which were modeled by the Delany-Bazley model [35]. The sound impedance of the aluminum-foam panels close to the wheel-rail interactions (green curves in Figure 16) was solved through a model proposed by H. LI [36] for single layer Aluminum-foam panels with a cavity

behind. Other boundaries were assumed acoustically rigid, and the ground was assumed totally reflecting by applying the image source approach.

Figure 17 shows the predicted insertion losses in the comparison with the measured results. At low

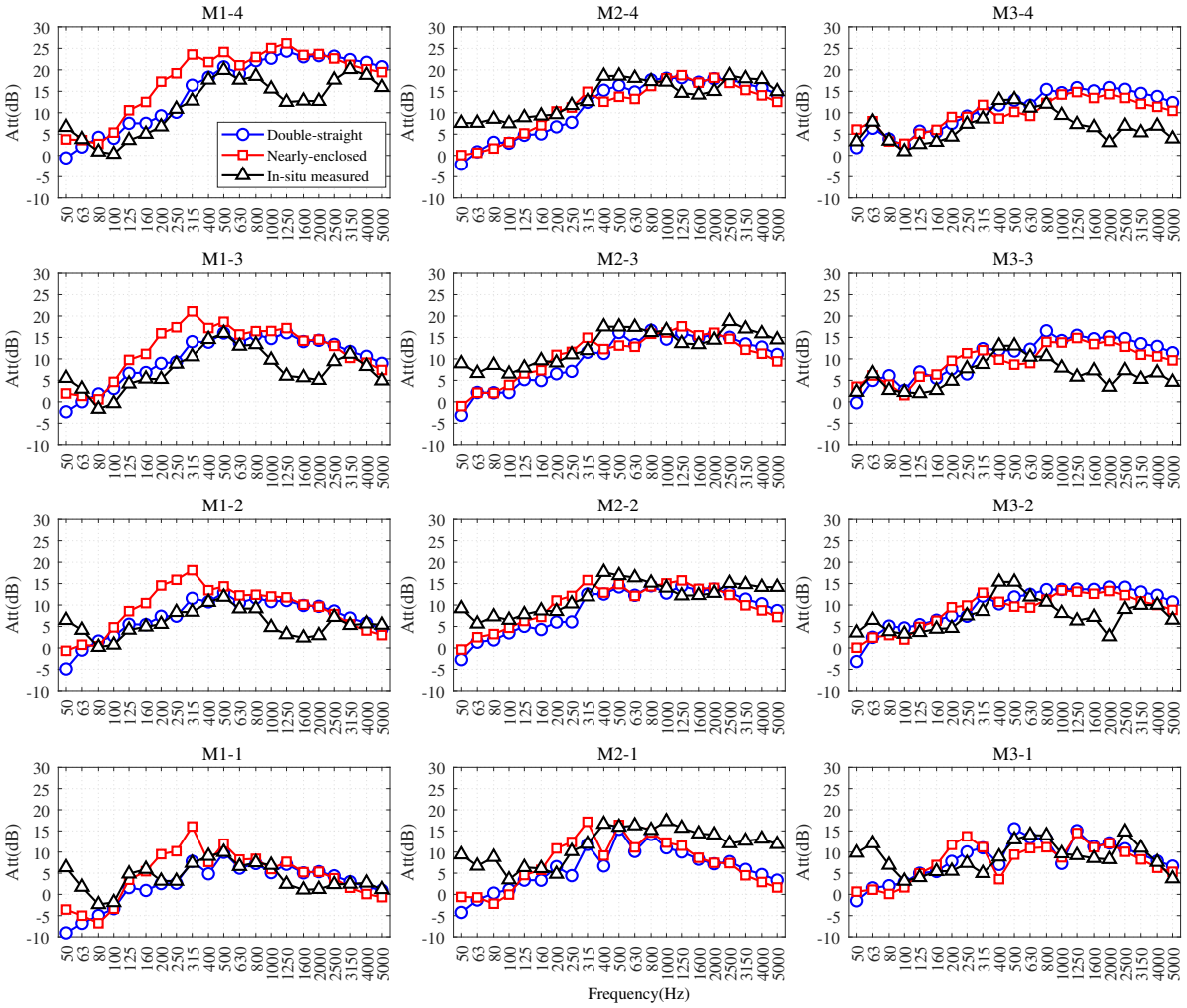


Figure 17: A comparison between predicted and measured results(red rectangular lines: predicted results for the nearly-enclosed barrier; blue circle lines: predicted results for the double-straight barrier; black triangle lines: measured results).

frequencies the measured results are higher than those predicted by the 2.5-D BEM models, consistent with the argument in Section 3.4.2. The values of the predicted insertion losses are almost equal to zero, or even negative, which confirms the previous thought that the nearly-enclosed barrier has a negative but small effect on low-frequency noise.

In the range of 125-400 Hz, the predicted insertion losses for the nearly-enclosed barrier overestimate the measured results but good agreements are observed between the predictions for the double-straight barrier and the measured results. A previous work [34] using scale model experiments and the 2.5-D BEM approach

concluded that noise radiated from the source inside the scale model could transmit noise through the top PC sheets with a thickness of 6 mm. Since the prototype has 6.5-mm-thick PC sheets at the top, the sound insulation property is seemingly not to be sufficient. The predicted transmission loss of the 6.5-mm-thick PC sheet from calculation in the diffuse sound field condition was utilized to compare with the predicted and measured insertion losses, as shown in Figure 18. It suggests that the PC sheets could not effectively

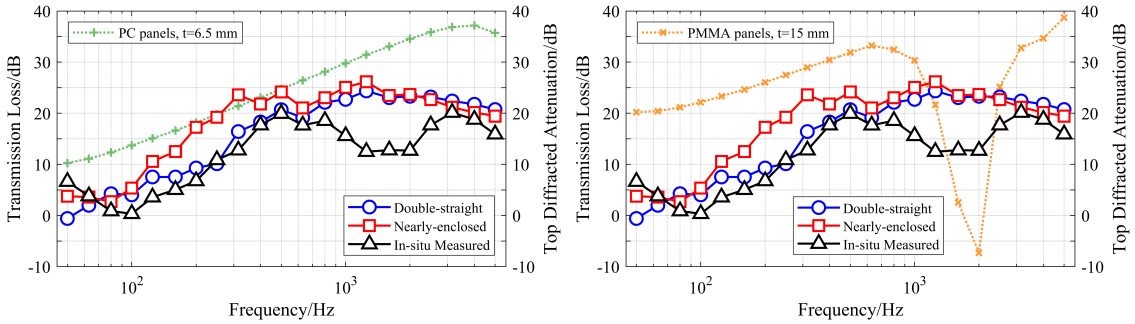


(a) Compared with transmission loss of PC panels (b) Compared with transmission loss of PMMA panels

Figure 18: One-third octave spectra for a comparison between measured and predicted insertion losses, and transmission loss of transparent panels (receiver M1-4)

insulate the sound since every transmission loss at 125-400 Hz is higher than the predicted insertion loss less than 5 dB. Thus, the PC sheets at the top can only play a role on an arch shape with a high flexibility and transparency, but have no significant effect on the sound insulation for URT noise, resulting in the overestimation of 2.5-D BEM predictions from 125 Hz to 400 Hz.

In the range of 500-800 Hz, there are good agreements between each two curves for each receiver position. However, at frequencies from 1000 Hz to 2500 Hz, there are remarkable differences between the predicted and measured results, especially for the receivers at a height close to that of the source (M-2, M-3, M-4). Based on the theory of sound insulation, these differences are probably from the coincident effect of the employed PMMA sheets. According to Equation (8.3) in [37], the critical frequency for the employed 15-mm-thick PMMA sheets was calculated as about 2000 Hz. Therefore, at the frequency of about 2000 Hz, the PMMA sheets would be strongly driven by the incident sound, and would radiate a corresponding acoustic wave well. Hence the transmission loss of the employed PMMA sheets was markedly reduced in this range (as shown in Figure 18(b)) and they can be considered as "transparent" sheets allowing exposure to URT noise. Nevertheless, at frequencies above 2000 Hz, the transmission loss rises again, approaching an extension of the original curve, in accordance with good agreements observed in Figure 17 between the predicted and measured results at each receiver position.

## 5. Conclusion

A series of in-situ measurements for a prototype of nearly-enclosed barrier were taken at twelve receiver positions. By using a piezoelectric acceleration sensor on a rail foot, the train speed for each pass-by was measured and the pass-by A-weighted level was therefore speed-corrected. A comparison of 2.5-D BEM predicted and measured results was also made to discuss the noise-reduced characteristics of the prototype. The results obtained allow the following conclusions to be drawn:

1. A positive correlation was found between the pass-by rail vertical acceleration level and train speed, and the other train speed dependence was found in the pass-by A-weighted level, in accordance with the prediction formula for rolling noise.
2. Most of the measured noise at the site without a barrier were much higher than the limit value (70 dB(A)) stated on the Chinese norm. The measured noise had a significant low and mid- frequency characteristics, with the structural-borne noise of the viaduct in the range of 50-200 Hz and the vehicle noise at 315-1000 Hz and 2000-4000 Hz.
3. The nearly-enclosed prototype provided the global insertion losses with a maximum of 17 dB(A), and a minimum of more than 6 dB(A). The insertion loss in the range of measured vehicle noise yielded on average more than 15 dB. But at low frequencies, caused by the resonance effect, the nearly-enclosed prototype had a negative but not remarkable effect.
4. The top PC sheets could not provide sufficient transmission losses, resulting in an overestimation of the predicted insertion losses in the range of 125-400 Hz. The employed PMMA sheets with a critical frequency of about 2000 Hz caused the coincidence effect, leading to the low measured insertion losses at 1000-2000 Hz.
5. Due to the poor sound insulation properties of the top PC sheets, the only significant gains compared with the double-straight barriers could not be obtained. Therefore, the nearly-enclosed barrier is a seriously efficient solution for attenuating urban rail traffic noise, but the economic benefits are not satisfactory.

## Acknowledgements

This work was sponsored by Shanghai Pujiang Program (20PJ1417300) and Shanghai Rising-Star Program (19QB1401100). The authors would like to acknowledge many people who were involved in this work. The authors also wish to thank China Scholarship Council and Ecole Nationale des Ponts et Chaussees, for providing necessary financial assistance to LI Qiutong to pursue her Ph. D. in France.

## References


[1] L. Yunfang, D. Lin, The Pollution Control of Urban Elevated Railway Traffic Noise, in: Euronoise2015, 2015, pp. 1683–1687.

[2] D. Zhang, J. Jiao, How Does Urban Rail Transit Influence Residential Property Values? Evidence from An Emerging Chinese Megacity, Sustainability 11 (2019) 534. doi:10.3390/su11020534.

[3] I. Ekici, H. Bougdah, A Review of Research on Environmental Noise Barriers, Building Acoustics (2004). doi:10.1260/135101003772776712.

[4] D. J. Oldham, C. A. Egan, A Parametric Investigation of the Performance of T-Profiled Highway Noise Barriers and the Identification of a Potential Predictive Approach, Applied Acoustics 72 (2011) 803–813. doi:10.1016/j.apacoust.2011.04.012.

[5] D. J. Oldham, C. A. Egan, A Parametric Investigation of the Performance of Multiple Edge Highway Noise Barriers and Proposals for Design Guidance, Applied Acoustics (2015). doi:10.1016/j.apacoust.2015.03.012.

[6] T. Ishizuka, K. Fujiwara, Performance of noise barriers with various edge shapes and acoustical conditions, Applied Acoustics 65 (2004) 125–141. doi:10.1016/j.apacoust.2003.08.006.

[7] J. Li, J. He, Acoustic Modelling of Noise Barrier Design for Fangshang Line in Urban Rail Transit in Beijing (in Chinese), Railway Standard Design 01 (2011) 104–106. doi:10.13238/j.issn.1004-2954.2011.01.034.

[8] Q. Zhao, M. Li, F. Zhou, X. Li, Noise Reduction Effects of Different Sound Barriers on Rail Transit Bridge (in Chinese), in: World Transport Convention, 2018, pp. 1526–1533.

[9] B. Shen, Detailed Design Scheme of Traffic Acoustic Barrier Project for a Tunnel (in Chinese), Urban Roads Bridges & Flood Control 04 (2019) 214–220.

[10] N. Ma, Design of Fully-closed Noise Barrier in Shanghai Rail Transit Line 6 (in Chinese), Modern Urban Transit 05 (2010) 38–39+5.

[11] N. Ma, Design of Fully-Closed Sound-Barrier Work for Shanghai Mingzhu Rail Transit Line (in Chinese), Modern Urban Transit 03 (2005) 41–42+6.

[12] G. R. Watts, P. A. Morgan, M. Surgand, Assessment of the Diffraction Efficiency of Novel Barrier Profiles Using an MLS-Based Approach, Journal of Sound and Vibration 274 (2004) 669–683. doi:10.1016/j.jsv.2003.05.005.

[13] P. Jean, Y. Gabillet, Using a Boundary Element Approach to Study Small Screens Close to Rails, Journal of Sound and Vibration 231 (2000) 673–679. doi:10.1006/jsvi.1999.2554.

[14] S. Sakamoto, A. Aoki, Numerical and Experimental Study on Noise Shielding Effect of Eaves/Louvers Attached on Building Façade, Building and Environment (2015). doi:10.1016/j.buildenv.2015.05.015.

[15] X. Wu, In-Situ Measurement on Noise Reduction Effect of Railway Fully-Enclosed Barrier (in Chinese), Railway Standard Design (2019).

[16] D. C. Hothersall, D. H. Crombie, S. N. Chandler-Wilde, The Performance of T-Profile and Associated Noise Barriers, Applied Acoustics 32 (1991) 269–287. doi:10.1016/0003-682X(91)90075-P.

[17] M. Baulac, J. Defrance, P. Jean, F. Minard, Efficiency of Noise Protections in Urban Areas: Predictions and Scale Model Measurements, Acta Acustica united with Acustica (2006).

[18] F. Koussa, J. Defrance, P. Jean, P. Blanc-Benon, Acoustic Performance of Gabions Noise Barriers: Numerical and Experimental Approaches, Applied Acoustics 74 (2013) 189–197. doi:10.1016/j.apacoust.2012.07.009.

[19] P. Jean, J. Defrance, Y. Gabillet, The Importance of Source Type on the Assessment of Noise Barriers, Journal of Sound and Vibration 226 (1999) 201–216. doi:10.1006/jsvi.1999.2273.

[20] Q. Li, D. Duhamel, H. Yin, Y. Luo, Comparative Analysis of Different Types of Sources on the Performance of Rigid Noise Barriers on Rigid Ground Using Analytical Formulae, a 2.5-D BEM Method and Scale Modelling Tests, Acta Acustica united with Acustica 105 (2019). doi:10.3813/AAA.919379.

[21] D. Duhamel, Efficient Calculation of the Three-Dimensional Sound Pressure Field Around a Noise Barrier, Journal of Sound and Vibration 197 (1996) 547–571. doi:10.1006/jsvi.1996.0548.

[22] D. Duhamel, P. Sergent, Sound Propagation over Noise Barriers with Absorbing Ground, Journal of Sound and Vibration (1998). doi:10.1006/jsvi.1998.2834.

[23] F. Dai, D. J. Thompson, Y. Zhu, X. Liu, Vibration Properties of Slab Track Installed on a Viaduct, Proceedings of the Institution of Mechanical Engineers, Part F: Journal of Rail and Rapid Transit (2016). doi:10.1177/0954409714533790.

[24] C. K. Hui, C. F. Ng, The Effects of Floating Slab Bending Resonances on the Vibration Isolation of Rail Viaduct, Applied Acoustics (2009). doi:10.1016/j.apacoust.2008.09.018.

[25] G. P. Wilson, Use of Floating Slab Track to Control Noise from Rail Transportation Systems, The Journal of the Acoustical Society of America (2012). doi:10.1121/1.4708190.

[26] ISO 10847:1997, Acoustics – In-situ Determination of Insertion Loss of Outdoor Noise Barriers of All Types, 1997.

[27] CEN/TS 16272-7:2015, Railway Applications - Track - Noise Barriers and Related Devices Acting on Airborne Sound Propagation - Test Method for Determining the Acoustic Performance - Part 7: Extrinsic Characteristics - In-situ Values of Insertion Loss, 2015.

[28] Q. Li, D. Duhamel, Y. Luo, H. Yin, Improved Methods for In-situ Measurement Railway Noise Barrier Insertion Loss, Transactions of Nanjing University of Aeronautics and Astronautics 35 (2018).

[29] S. I. Voropayev, N. C. Ovenden, H. J. S. Fernando, P. R. Donovan, Finding Optimal Geometries for Noise Barrier Tops Using Scaled Experiments, The Journal of the Acoustical Society of America 141 (2017) 722–736. doi:10.1121/1.4974070.

[30] A. Jolibois, J. Defrance, H. Koreneff, P. Jean, D. Duhamel, V. W. Sparrow, In Situ Measurement of the Acoustic Performance of A Full Scale Tramway Low Height Noise Barrier Prototype, Applied Acoustics 94 (2015) 57–68. doi:10.1016/j.apacoust.2015.02.006.

[31] F. Poisson, P. E. Gautier, F. Letourneaux, Noise Sources for High Speed Trains: A Review of Results in the TGV Case, in: Notes on Numerical Fluid Mechanics and Multidisciplinary Design, 2008, pp. 71–77.

[32] GB 3096-2008, Environmental quality standard for noise(in Chinese), 2008.

[33] J. Sadeghi, A. Hasheminezhad, Correlation Between Rolling Noise Generation and Rail Roughness of Tangent Tracks and Curves in Time and Frequency Domains, Applied Acoustics (2016). doi:10.1016/j.apacoust.2016.01.006.

[34] Q. Li, D. Duhamel, Y. Luo, H. Yin, Analyzing the Acoustic Performance of a Nearly-Enclosed Noise Barrier Using Scale Model Experiments and a 2.5-D BEM Approach, Applied Acoustics 158 (2020). doi:10.1016/j.apacoust.2019.107079.

[35] M. E. Delany, E. N. Bazley, Acoustical Properties of Fibrous Absorbent Materials, Applied Acoustics (1970). doi:10.1016/0003-682X(70)90031-9.

[36] H. LI, Study on Sound Absorption Behavior of Metal Foam, Ph.D. thesis, North China Electric Power University, 2009.

[37] D. A. Bies, C. Hansen, C. Howard, Engineering Noise Control : Theory and Practice, CRC Press, Boca Raton, FL, USA, 2009.